geosciences

MDPI

Article

Machine Learning Insights into the Last 400 Years of Etna Lateral Eruptions from Historical Volcanological Data

Arianna Beatrice Malaguti, Claudia Corradino, Alessandro La Spina, Stefano Branca and Ciro Del Negro *

Istituto Nazionale di Geofisica e Vulcanologia, Sezione di Catania, Osservatorio Etneo, 95125 Catania, Italy; arianna.malaguti@ingv.it (A.B.M.); claudia.corradino@ingv.it (C.C.); alessandro.laspina@ingv.it (A.L.S.); stefano.branca@ingv.it (S.B.)

* Correspondence: ciro.delnegro@ingv.it

Abstract: Volcanic hazard assessment is generally based on past eruptive behavior, assuming that previous activity is representative of future activity. Hazard assessment can be supported by Artificial Intelligence (AI) techniques, such as machine learning, which are used for data exploration to identify features of interest in the data. Here, we applied a machine learning technique to automate the analysis of these datasets, handling intricate patterns that are not easily captured by explicit commands. Using the k-means clustering algorithm, we classified effusive eruptions of Mount Etna over the past 400 years based on key parameters, including lava volume, Mean Output Rate (MOR), and eruption duration. Our analysis identified six distinct eruption clusters, each characterized by unique eruption dynamics. Furthermore, spatial analysis revealed significant sectoral variations in eruption activity across Etna's flanks. These findings, derived through unsupervised learning, offer new insights into Etna's eruptive behavior and contribute to the development of hazard maps that are essential for long-term spatial planning and risk mitigation.

Keywords: machine learning; artificial intelligence; Etna volcano; effusive eruptions; volcanic hazard; K-means clustering

Citation: Malaguti, A.B.; Corradino, C.; La Spina, A.; Branca, S.; Del Negro, C. Machine Learning Insights into the Last 400 Years of Etna Lateral Eruptions from Historical Volcanological Data. *Geosciences* **2024**, *14*, 295. https://doi.org/10.3390/geosciences14110295

Academic Editors: Ian Coulson and Fei Wang

Received: 12 September 2024
Revised: 25 October 2024
Accepted: 1 November 2024
Published: 3 November 2024

1. Introduction

Volcanoes are complex dynamic systems, and understanding their activity at any given time poses an ongoing challenge, particularly for frequently erupting volcanoes in densely populated areas. One such case is Mount Etna (Sicily, Italy), where lava flows present the primary hazard. Although less frequent than explosive events, lava flows can have significant socio-economic impacts, especially given the densely populated areas surrounding the volcano. Over the past century, several large flank eruptions have caused extensive damage to agricultural land and disrupted towns and villages [1–3]. A marked increase in both eruption frequency and lava production has been observed since 1971 [4–7], with 20 major flank eruptions occurring along two prominent fracture zones trending south and northeast. This activity highlights the persistent threat posed by Etna's eruptive behavior over the past 40 years [6,8].

Recent advances in Artificial Intelligence (AI) have greatly enhanced our ability to monitor, analyze, and predict volcanic processes, ultimately improving risk management and the protection of communities in hazard-prone regions. Machine Learning (ML), a key subset of AI, has transformed volcanology by enabling the analysis of vast and complex datasets from a wide range of sensors. These include data on ground deformation, seismic activity, geomagnetic and electromagnetic variations, and thermal anomalies, processed with high levels of accuracy [9–26]. Furthermore, ML algorithms can automatically analyze satellite imagery and aerial photographs to detect morphological changes in volcanoes, such as the formation of new vents, the collapse of crater walls, or the development of lava flow paths [13]. These capabilities allow for the real-time processing of data streams

from monitoring stations, providing early warnings of impending eruptions and enabling real-time volcanic risk assessments [9–14].

In particular, machine learning techniques have proven invaluable for handling large volcanic datasets to uncover hidden patterns and extract meaningful insights [27–29]. Unsupervised learning models, which do not require explicit instructions, are particularly suited for analyzing the complex, multi-dimensional data associated with volcanic activity [18,30–32]. These models can learn the underlying structure of the data, helping to elucidate the dynamics of historical eruptions based on geophysical and volcanological observations (e.g., ground deformation and seismic events).

At the Etna Volcano Observatory (EVO), a continuous flow of geophysical and volcanological data is used to deepen our understanding of volcanic processes and improve our ability to identify signs of volcanic unrest, forecast eruptions, and assess hazards. Here, we apply Cluster Analysis (CA), an unsupervised learning approach, to classify Etna's flank eruptions over the past 400 years. This technique groups similar eruptions and distinguishes those with different characteristics, providing new insights into the eruptive dynamics of Mount Etna's volcanic system.

2. Etna Flank Eruptions

Mount Etna is a basaltic stratovolcano located along the Ionian coast of eastern Sicily, Italy (Figure 1), known for its persistent activity [33,34]. This activity includes continuous degassing, intermittent Strombolian eruptions, and more violent explosive events at its summit craters [35]. Frequent flank eruptions, characterized by lava flows and often accompanied by weak explosive activity, and rarer eccentric eruptions also define its eruptive behavior [2,35–38]. While summit eruptions are relatively frequent [2,36,37,39–42], lateral eruptions occur less often, with intervals of several years between events [2,37].

Etna's eruptive history over the past three millennia is documented in historical sources, making it a unique case globally. However, comprehensive and accurate documentation of flank eruptions begins only after the mid-17th century [2,37,43], while the catalog of summit activity becomes reliable in the late 19th century [44]. Historical analyses, such as those by Branca and Del Carlo [2], indicate that following the major 1669 eruption, a period of reduced volcanic activity ensued. This pattern shifted after 1763, with a notable increase in flank activity, peaking between 1961 and 2003, when the frequency of eruptions quadrupled compared to earlier periods [37].

Geological data suggest that summit eruptions are generally more frequent than flank eruptions [12,45]. However, flank eruptions pose a greater hazard due to the dense population surrounding Etna [11,12]. In the last 400 years, the most destructive eruption occurred in 1669 [46]. In the 20th century, the town of Mascali was almost completely destroyed by lava flows in 1928 [47], and towns such as Fornazzo, Randazzo, and Zafferana Etnea were threatened in 1971, 1981, and 1992, respectively [48–51]. More recently, the 2001 and 2002–2003 eruptions caused significant damage to tourist facilities in the summit area [52–56].

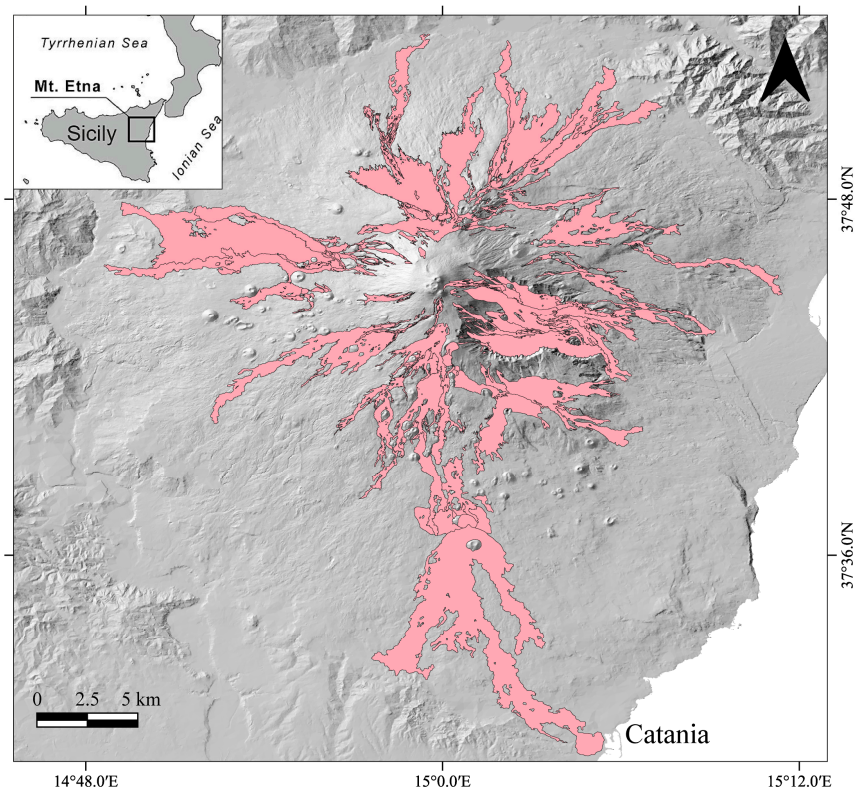

Figure 1. Sketch map of Etna flank lava flows over the last 400 years from historical catalogs [2,38,57–60]. The shaded relief image was derived from the 10 m resolution TINITALY DEM [61].

3. Data Analysis

This study focuses on Etna's flank eruptions from 1610 to 2019 (Figure 1 and Table 1), drawing primarily on historical catalogs that document 60 lateral eruptions [2,38,57–60]. These catalogs provide detailed information on eruption duration, lava volumes, and the spatial distribution of past effusive events.

We analyzed the temporal distribution of these lateral eruptions over the past 400 years, focusing on their duration, lava volume, and the position of effusive vents (or fissures) to identify distinct eruptive clusters. The Mean Output Rate (MOR) was also calculated by dividing the final volume of erupted lava by the total duration of each eruption (Table 1). The use of MOR allows for better discrimination of the subclasses previously considered in studies, e.g., [62], as it characterizes eruptions independently of nominal volume or duration, shedding light on the different effusive dynamics of eruptive episodes. Relying solely on duration and volume intervals does not fully capture these effusive dynamics. This approach allowed us to classify the eruptions and better understand the varying dynamics of Etna's flank activity over the centuries.

Table 1. Summary of the main flank eruptions from 1669 to 2019 from historical catalogs [2,38,57–60].

Starting Year	Duration (Days)	Volume (Mm^3)	MOR (Mm^3/day)
30 May 2019	8	4.4	0.55
24 December 2018	2	4.25	2.12
4 September 2008	419	77	0.18
7 September 2004	182	40	0.21
27 October 2002	93	30	0.32
27 October 2002	8	10	1.25
17 July 2001	23	20	0.86
14 December 1991	473	235	0.49

Table 1. *Cont.*

Starting Year	Duration (Days)	Volume (Mm^3)	MOR (Mm^3/day)
27 October 1989	10	26	2.6
30 October 1986	122	60	0.49
25 December 1985	3	0.8	0.26
12 March 1985	125	30	0.24
28 March 1983	131	79	0.60
17 March 1981	6	22	3.66
3 August 1979	6	7.5	1.25
18 November 1978	12	11	0.91
24 August 1978	6	4	0.66
29 April 1978	37	27	0.72
24 February 1975	187	6	0.03
11 March 1974	18	2.1	0.11
30 January 1974	17	2.4	0.14
5 April 1971	69	45	0.65
7 January 1968	117	1	0.008
25 November 1950	372	151	0.40
2 December 1949	3	12	4
30 June 1942	1	1.6	1.6
2 November 1928	18	52	2.88
17 June 1923	31	78	2.51
30 November 1918	2	1.2	0.6
10 September 1911	13	55	4.23
23 March 1910	26	65	2.5
29 April 1908	1	2	2
9 July 1892	173	121	0.69
19 May 1886	20	38	1.9
22 March 1883	3	0.2	0.06
26 May 1879	12	22	1.83
29 August 1874	2	1.5	0.75
30 January 1865	150	30	0.2
20 August 1852	280	87	0.31
17 November 1843	11	52	4.72
31 October 1832	23	50	2.17
25 May 1819	70	47	0.67
27 October 1811	182	51	0.28
27 March 1809	14	36	2.57
15 November 1802	3	10	3.33
26 May 1792	380	90	0.23
18 May 1780	10	29	2.9
27 April 1766	194	135	0.69
18 June 1763	84	100	1.19
6 February 1763	32	19	0.59
9 March 1755	6	4.7	0.78
8 March 1702	60	17	0.28
11 March 1669	122	600	4.91
14 March 1689	30	20	0.66
18 July 1643	10	4	0.4
January 1651–December 1654	1095	475	0.43
20 November 1646–1647	58	153	2.63
19 December 1634–June 1636	530	203	0.38
1 June 1614–1624	3650	1070	0.29
3 May 1610-July 1610	90	120	1.33

4. Method

A detailed classification based on lava volumes, MOR, and the duration of these effusive eruptions was performed using the k-means function in MATLAB. Volcanic features are given as input to an unsupervised learning algorithm to group similar data, where similarity is evaluated quantitatively using a distance function in the space of feature

vectors. We chose the non-hierarchical k-means algorithm because it is simple and efficient. It is an iterative procedure that partitions data into a predetermined number of clusters. Firstly, inside the feature space, cluster centroids are randomly initialized, and observations are assigned to the nearest centroid according to the cosine distance. The cosine distance is one minus the cosine of the included angle between feature vectors. Secondly, cluster centroids are updated with the mean location within their cluster. These steps are repeated until an optimal convergence is reached. A cluster analysis using the k-means algorithm was applied to the normalized input data, i.e., z-score normalization is needed to scale the data and reduce variability across arrays [63].

A critical parameter in the k-means clustering algorithm is the number of clusters, k. Estimating k can be challenging as it depends on the data's complexity and the desired resolution. Too many clusters can complicate interpretation, while too few may overlook significant patterns. When the optimal number of clusters is not known beforehand, three common techniques can help determine k: (1) the elbow method, e.g., [64,65]; (2) the gap statistic, e.g., [31,66,67]; and (3) the silhouette method, e.g., [68,69]. These methods involve performing k-means clustering for a range of k values and computing different metrics to identify the optimal k.

We used the elbow method to find the right number of clusters. The elbow method is a graphical routine for finding the optimal K value in a k-means clustering algorithm. The elbow graph shows the within-cluster sum-of-square (WCSS) values on the *y*-axis corresponding to the different values of k (on the *x*-axis). The optimal k value is the point at which the graph forms an elbow.

5. Results

Using the elbow method, the optimal number of clusters to be set is six (Figure 2). Thus, a k-means clustering defining k = 6 is applied to the entire dataset. The centroids (duration, volume, MOR) of the randomly initialized clusters can be seen in Table 2. By combining these considerations on the distributions of the durations, volumes, and MOR, six eruptive classes can be defined (see also Tables 2 and 3; Figure 3):

- Cluster 1 is characterized by eruptions of short duration, low lava volume, and high MOR (Tables 2 and 3; Figure 3a,b).
- Cluster 2 is characterized by a very low MOR, high duration, and low lava volume (Tables 2 and 3; Figure 3a).
- Cluster 3 is characterized by low volume and low duration but medium to high MOR (Tables 2 and 3; Figure 3a,b).
- Cluster 4 is characterized by a high volume, high duration, and low MOR (Tables 2 and 3; Figure 3a).
- Cluster 5 is characterized by medium duration, high lava volume, and high MOR (Tables 2 and 3; Figure 3a).
- Cluster 6 is characterized by eruptions of short duration, low volume, and low MOR (Tables 2 and 3; Figure 3a).

We also investigated the spatial distribution of these past effusive events. The boundary angles for each sector were determined using the zeros and minima of the fissure orientation distribution over the last 15,000 years [70]. Following the analysis by Duncan et al. [71], the sectors are defined as follows: Sector 1 spans from 355° to 115°, Sector 2 extends from 115° to 225°, and Sector 3 ranges from 225° to 355°. Thus, we divided the Etna area into three different sectors: the E-S, N-E, and W sectors (Figure 4):

- Clusters 1 and 3 affect all three Etna sectors, with greater incidence in the E-S and N-E flanks of Etna (Figure 4a,c).
- Cluster 2 includes events that occurred in the E-S sector, except for three episodes (Figure 4b).
- Cluster 4 is characterized by eruptive events that occurred mostly in the E-S sector of Etna, except for one eruption in the N-NE sector and another one in the W sector (Figure 4d).

- Cluster 5 includes events that occurred in the E-S and W sectors (Figure 4e).
- Cluster 6 is characterized by two events located in the E-S sector and one eruption in the N-NE sector (Figure 4f).

In addition, the number of eruptive episodes within the six clusters across the three sectors was analyzed and is illustrated in Figure 5. This allows for the identification of the most recurrent clusters, which differ between the various sectors.

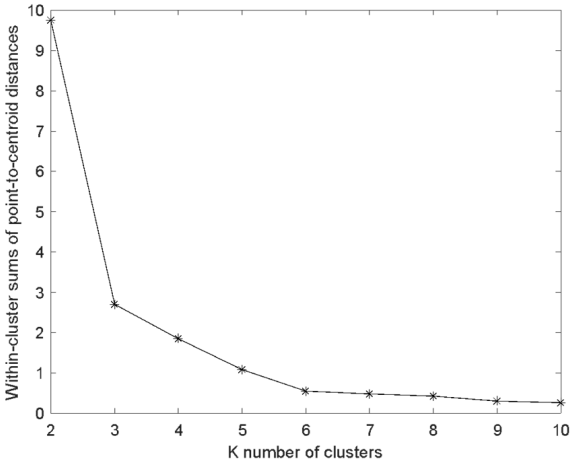

Figure 2. Elbow graph showing the within-cluster sum-of-square (WCSS) values on the *y*-axis corresponding to the different values of K (on the *x*-axis).

Table 2. Centroids for each cluster.

Clusters	Duration	Volume	MOR
K1	15.3	41.5	2.8
K2	197.3	48.4	0.3
K3	22.6	12.85	0.5
K4	926.7	341.4	0.5
K5	98.7	273.3	2.5
K6	5	6.4	1.4

Table 3. Cluster subdivision of Etna's lateral eruptions.

Starting Year	Clusters	Starting Year	Clusters
24 December 2018	1	17 July 2001	3
27 October 1989	1	25 December 1985	3
17 March 1981	1	18 November 1978	3
2 December 1949	1	24 August 1978	3
2 November 1928	1	29 April 1978	3
17 June 1923	1	11 March 1974	3
10 September 1911	1	30 January 1974	3
23 March 1910	1	5 April 1971	3
29 April 1908	1	30 November 1918	3
19 May 1886	1	22 March 1883	3
26 May 1879	1	29 August 1874	3
17 November 1843	1	25 May 1819	3
31 October 1832	1	6 February 1763	3
27 March 1809	1	9 March 1755	3
15 November 1802	1	8 March 1702	3
18 May 1780	1	14 March 1689	3

Table 3. *Cont.*

Starting Year	Clusters	Starting Year	Clusters
20 November 1646–1647	1	18 July 1643	3
4 September 2008	2	14 December 1991	4
7 September 2004	2	25 November 1950	4
27 October 2002	2	9 July 1892	4
30 October 1986	2	27 April 1766	4
12 March 1985	2	January 1651–December 1654	4
28 March 1983	2	19 December 1634–June 1636	4
24 February 1975	2	1 June 1614–1624	4
7 January 1968	2	18 June 1763	5
30 January 1865	2	11 March 1669	5
20 August 1852	2	3 May 1610-July	5
27 October 1811	2	27 October 2002	6
26 May 1792	2	3 August 1979	6
30 May 2019	3	30 June 1942	6

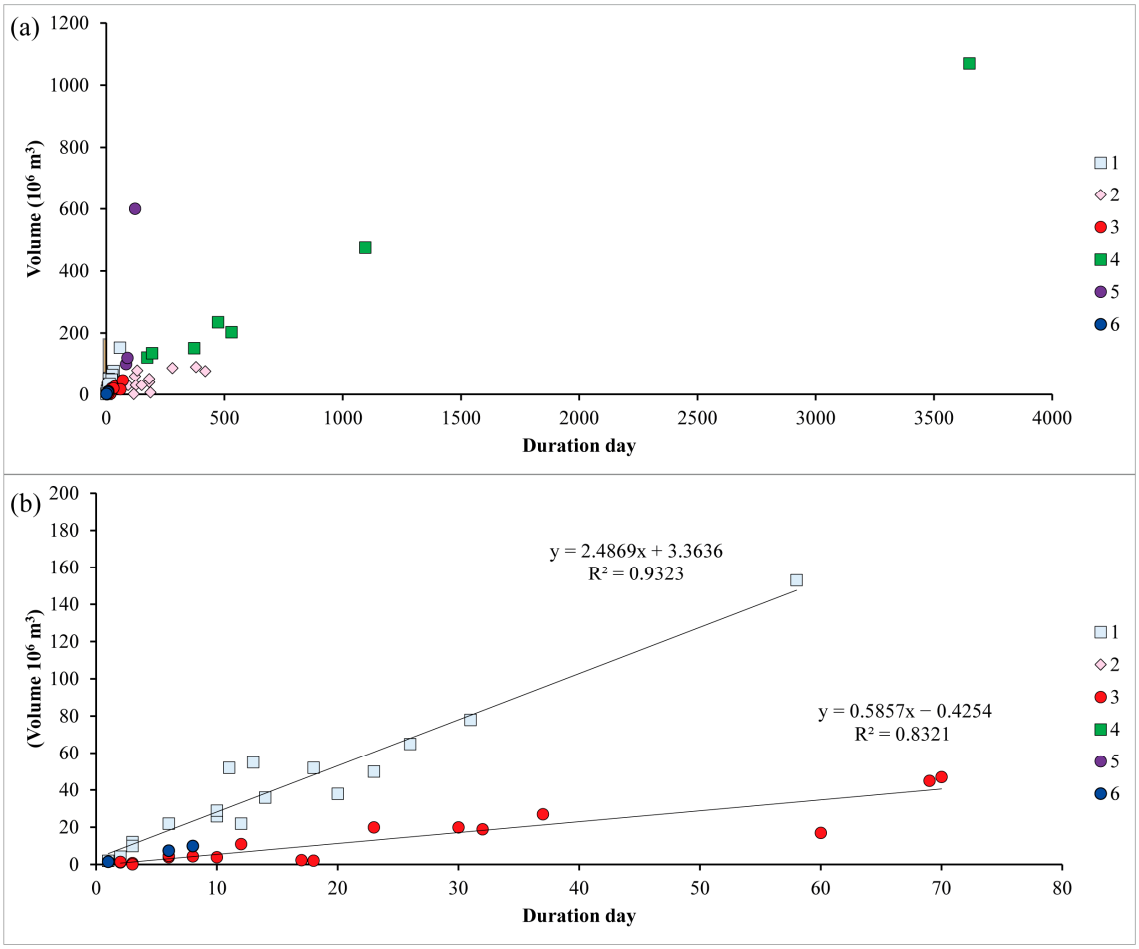

Figure 3. (**a**) Distribution of durations, MOR, and volumes of the 60 lava flows and their subdivision into six clusters. (**b**) Detail of clusters 1, 3, and 6.

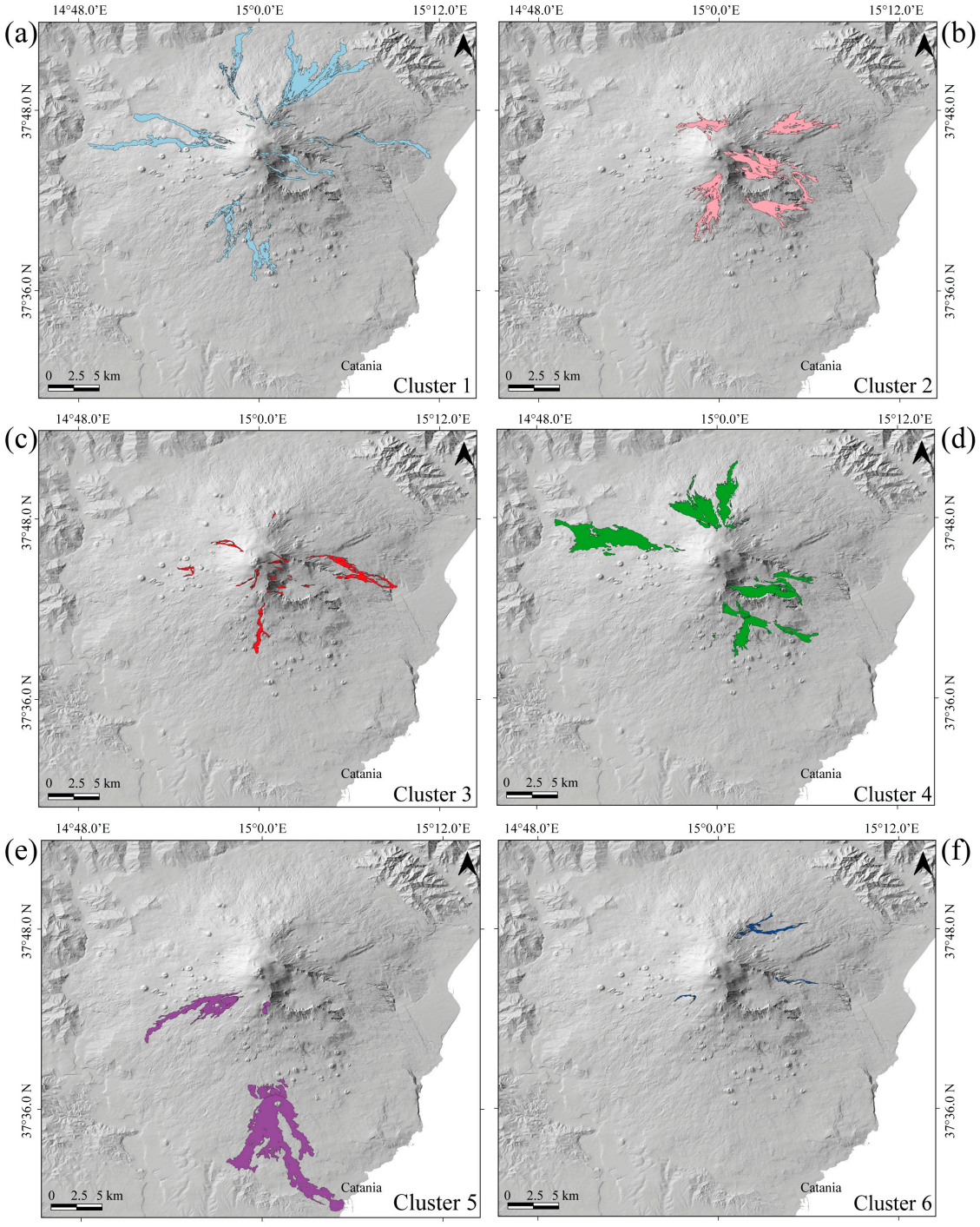

Figure 4. Sketch map of Etna flank lava flows over the last 400 years from historical data [2,38,57–60], subdivided according to the six clusters identified. The shaded relief image was derived from the 10 m resolution TINITALY DEM [61]. (**a**) Cluster 1 events are mainly located in the N-NE sector, with some occurrences in the E-S and W sectors; (**b**) Most of the Cluster 2 events occurred in the E-S sector, with some exceptions in the NE sector; (**c**) Cluster 3 is distributed across the E-S and W sectors; (**d**) Cluster 4 eruptions are mostly concentrated in the E-S sector, with a few exceptions in the NE and W sectors; (**e**) Cluster 5 includes eruptions located in the E-S sector, except for one event in the W sector; (**f**) Cluster 6 includes events located in the E-S and NE sectors.

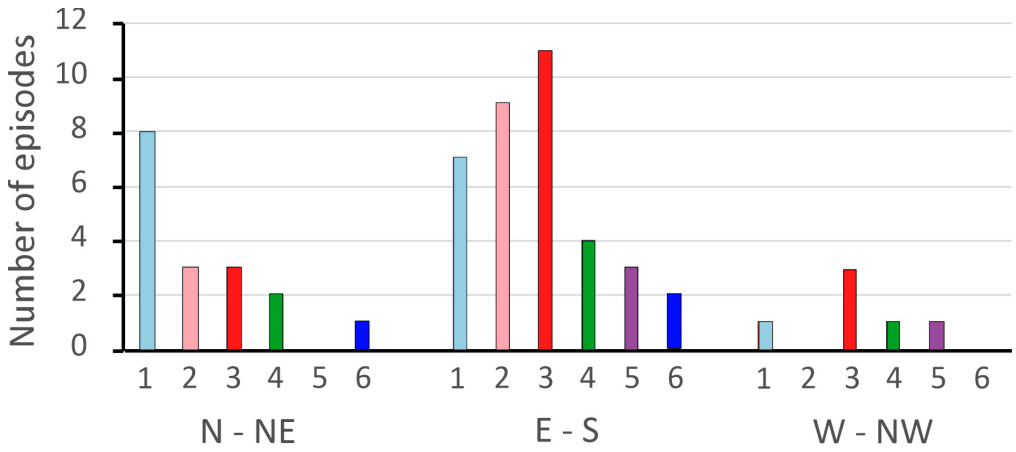

Figure 5. Distributions of the six clusters in the three sectors into which Etna was divided.

6. Discussion

The use of unsupervised learning enabled the classification of Etna's flank eruptions over the last 400 years into six distinct clusters based on duration, lava volume, and MOR (Figure 3; Tables 1 and 3). Clusters 1 and 3 share similarities in terms of short eruption durations (<35 days) and low lava volumes (<80 Mm^3), but the inclusion of MOR and the clustering technique allowed us to distinguish between them (Figure 3b). Cluster 1 has a significantly higher MOR (2.8 Mm^3/day) compared to Cluster 3 (0.5 Mm^3/day), indicating different eruptive behaviors despite similar duration and volume. From a volcanological perspective, these clusters correspond to two types of activity defined by Branca and Del Carlo [37]. Cluster 1 is associated with Strombolian activity limited to the early stages of lava effusion, producing hornitos and small scoria cones, consistent with Class A eruptions. In contrast, Cluster 3 represents more explosive eruptions, often extending until the end of lava effusion, characteristic of Class B eruptions, which include vigorous strombolian and lava-fountaining activity.

The two eruptive classes reflect distinct mechanisms. Class A eruptions (Cluster 1) involve magmas that have undergone multi-stage decompression and volatile loss before reaching the surface [72,73]. Meanwhile, Class B eruptions (Cluster 3) are fed by magma rising from deeper levels, retaining higher volatile content [73]. Spatially, Cluster 1 events are predominantly located in the N-NE sector, with a few occurrences in the E-S and W sectors (Figure 4a). In contrast, Cluster 3 events are distributed across the E-S and W sectors (Figure 4c), with notable examples such as the formation of Mt. De Fiore (1974 [74,75]) and Mt. Nuovo (1763 [75]) in the W sector and the 1874 eruption in the N sector [76].

Cluster 2, comprising 12 eruptions, is defined by intermediate durations (90–187 days) and volumes (30–80 Mm^3). Most of these events occurred in the E-S sector, with three exceptions in the NE sector (Figure 4b). Cluster 4 includes longer-duration eruptions (173 to 530 days, up to 3650 days in one case) and large volumes (120 to 1070 Mm^3). These eruptions are mostly concentrated in the E-S sector, with a few exceptions in the NE and W sectors (Figure 4d). Cluster 5 includes three notable eruptions with volumes between 100 and 120 Mm^3 and durations of 80–90 days, with the exception of the 1669 eruption, which lasted 122 days and produced 600 Mm^3 of lava. These eruptions are primarily located in the E-S sector, except for the 1610 eruption, which occurred in the W sector (Figure 4e [62]). Finally, Cluster 6 represents three short-duration events (6–9 days) with low volumes (7–10 Mm^3), with the exception of the 1942 eruption [2], which lasted just one day and had a volume of 2 Mm^3. Two of these events occurred in the E-S sector, while one (the October 2002 eruption) took place in the NE sector (Figure 4f).

The differences between Clusters 2, 4, 5, and 6 are explained by variations in the driving and lithostatic pressures, as well as the thermal evolution of the magma and host rock. Bruce and Huppert [77] proposed that during an eruption, the driving pressure decreases over time, reducing the flow rate. High-volume eruptions (>100 Mm^3) tend to

have longer durations (over 170 days) and lower average flow rates (under 6 m^3/s), as eruptions falling into Clusters 4 and 5, indicating a steady discharge maintained by the balance between internal dike pressure and lithostatic pressure, with cooling eventually closing the dike [78]. Shorter eruptions (<45 days; Clusters 2 and 6) likely result from insufficient internal pressure, while short-lived but high-volume eruptions are driven by high initial pressures.

A sectoral analysis of the volcano (Figure 5), considering three radial sectors (N-NE, E-S, and W), revealed that the N-NE sector is primarily characterized by Cluster 1 events. Both Clusters 2 and 3 also occur here, though Cluster 5 is absent. The E-S sector includes all six clusters, with Cluster 3 being the most prevalent, followed by Clusters 2 and 1. In the W sector, fewer events have occurred, and only Clusters 1, 3, 4, and 5 are present. The concentration of eruptions in the N-NE and E-S sectors suggests that these areas, particularly the densely inhabited eastern flanks, are at greater risk and should be the focus of hazard assessments.

7. Conclusions

The application of the k-means unsupervised machine learning algorithm, combined with MOR, lava volume, and eruption duration data, has yielded new insights into the eruptive behavior of Etna over the last 400 years. This clustering method identified, for the first time, two groups with similar eruption durations and volumes but differing MOR values. Cluster 1 is associated with Strombolian activity, primarily occurring during the early stages of lava effusion, leading to the formation of hornitos and small scoria cones (Class A of Branca and Del Carlo [37]). In contrast, Cluster 3 represents more explosive eruptions (Class B of Branca and Del Carlo [37]). The remaining clusters (2, 4, 5, and 6) exhibit variations in duration and volume, which are related to differences in eruptive pressures and magma evolution. This demonstrates the capability of unsupervised machine learning techniques to discern nuanced patterns in volcanic data that may not be immediately evident through traditional methods.

Sectoral analysis of the volcano indicates that the N-NE sector is predominantly represented by Cluster 1, with Clusters 2 and 3 also present, while Cluster 5 is absent. The E-S sector contains all six clusters, with Cluster 3 being the most frequent, followed by Clusters 2 and 1. In contrast, the W sector has fewer events, comprising only Clusters 1, 3, 4, and 5. This analysis reveals that the N-SE and S flanks have been more volcanically active compared to the N-SW flank. Notably, the E-S sector is characterized by eruptions with low duration, low lava volume, and medium to high MOR (Clusters 1 and 3), setting it apart from other sectors. Over the past 400 years, flank eruptions have primarily been concentrated in the densely populated eastern flanks, indicating a higher hazard for these areas. Consequently, these regions should be prioritized in volcanic risk assessments.

Because volcanic hazard assessment is generally based on past eruptive behavior, assuming that previous activity is representative of future activity, the characterization of duration, volume distributions, and MOR, as well as the spatial distributions of these past lateral eruptions, are essential to define the input for numerical simulations. These simulations can then be used to create more accurate volcanic hazard maps. Thus, the identification of these clusters not only enhances our understanding of Etna's eruptive history but also provides a foundation for improving hazard maps. These maps are crucial for long-term planning and risk mitigation, especially in highly populated areas on Etna's eastern slopes.

Our findings emphasize the importance of incorporating historical volcanological parameters—such as MOR, volume, and duration—into hazard assessment frameworks, providing a more comprehensive perspective of volcanic risk.

Author Contributions: Conceptualization, A.B.M. and C.C.; methodology, C.C.; software, A.B.M. and C.C.; validation, S.B.; formal analysis, A.B.M., C.C. and A.L.S.; data curation, A.B.M., C.C. and A.L.S.; writing—original draft preparation, A.B.M. and C.C.; writing—review and editing, A.L.S., S.B. and C.D.N.; visualization, A.B.M.; supervision, C.D.N.; project administration, C.D.N.; funding acquisition, C.D.N. All authors have read and agreed to the published version of the manuscript.

Funding: This research was funded by the ATHOS Research Programme (INGV OB.FU. 0867.010), by the 2019 Strategic Project FIRST—Forecasting Eruptive activity at Stromboli volcano: timing, eruptive style, size, intensity, and duration—of the INGV Volcanoes Department (Delibera n. 144/2020), and by Project INGV Pianeta Dinamico VT_ORME 2023–2025 (INGV OB.FU. 1020.010).

Data Availability Statement: All data used in this article are available in the tables in this article.

Acknowledgments: This work was developed within the framework of the Laboratory of Technologies for Volcanology (TechnoLab) at the INGV in Catania (Italy).

Conflicts of Interest: The authors declare no conflicts of interest. The funders had no role in the design of the study; in the collection, analyses, or interpretation of data; in the writing of the manuscript; or in the decision to publish the results.

References

1. Chester, D.K.; Duncan, A.M.; Dibben, C.; Guest, J.E.; Lister, P.H. Mascali, Mount Etna region Sicily: An example of fascist planning during the 1928 eruption and its continuing legacy. *Nat. Hazards* **1999**, *19*, 29–46. [CrossRef]
2. Branca, S.; Del Carlo, P. Eruptions of Mt Etna during the past 3200 years: A revised compilation integrating the Historical and stratigraphic records. In *Mt. Etna: Volcano Laboratory*; American Geophysical Union: Washington, DC, USA, 2004; pp. 1–27.
3. Bonaccorso, A.; Calvari, S.; Boschi, E. Hazard mitigation and crisis management during major flank eruptions at Etna volcano: Reporting on real experience. *Geol. Soc. Lond. Spec. Publ.* **2016**, *426*, 447–461. [CrossRef]
4. Wadge, G.; Guest, J.E. Steady-state magma discharge at Etna 1971–1981. *Nature* **1981**, *294*, 548–550. [CrossRef]
5. Smethurst, L.; James, M.R.; Pinkerton, H.; Tawn, J.A. A statistical analysis of eruptive activity on Mount Etna, Sicily. *Geophys. J. Int.* **2009**, *179*, 655–666. [CrossRef]
6. Harris, A.; Steffke, A.; Calvari, S.; Spampinato, L. Thirty years of satellite-derived lava discharge rates at Etna: Implications for steady volumetric output. *J. Geophys. Res. Solid Earth* **2011**, *116*, B08204. [CrossRef]
7. Andronico, D.; Lodato, L. Effusive activity at Mount Etna volcano (Italy) during the 20th century: A contribution to volcanic hazard assessment. *Nat. Hazards* **2005**, *36*, 407–443. [CrossRef]
8. Bonaccorso, A.; Calvari, S. Major effusive eruptions and recent lava fountains: Balance between expected and erupted magma volumes at Etna volcano. *Geophys. Res. Lett.* **2013**, *40*, 6069–6073. [CrossRef]
9. Currenti, G.; Del Negro, C.; Lapenna, V.; Telesca, L. Multifractality in local geomagnetic field at Etna volcano, Sicily (southern Italy). *Nat. Hazards Earth Syst. Sci.* **2005**, *5*, 555–559. [CrossRef]
10. Cappello, A.; Neri, M.; Acocella, V.; Gallo, G.; Vicari, A.; Del Negro, C. Spatial vent opening probability map of Etna volcano (Sicily, Italy). *Bull. Volcanol.* **2012**, *74*, 2083–2094. [CrossRef]
11. Cappello, A.; Bilotta, G.; Neri, M.; Negro, C.D. Probabilistic modeling of future volcanic eruptions at Mount Etna. *J. Geophys. Res. Solid Earth* **2013**, *118*, 1925–1935. [CrossRef]
12. Del Negro, C.; Cappello, A.; Neri, M.; Bilotta, G.; Hérault, A.; Ganci, G. Lava flow hazards at Mount Etna: Constraints imposed by eruptive history and numerical simulations. *Sci. Rep.* **2013**, *3*, 3493. [CrossRef]
13. Del Negro, C.; Cappello, A.; Ganci, G. Quantifying lava flow hazards in response to effusive eruption. *Bulletin* **2016**, *128*, 752–763. [CrossRef]
14. Del Negro, C.; Cappello, A.; Bilotta, G.; Ganci, G.; Hérault, A.; Zago, V. Living at the edge of an active volcano: Risk from lava flows on Mt. Etna. *Geol. Soc. Am. Bull.* **2020**, *132*, 1615–1625. [CrossRef]
15. Ebmeier, S.; Biggs, J.; Poland, M.; Pritchard, M.; Zoffoli, S.; Furtney, M.; Reath, K. Satellite geodesy for volcano monitoring in the Sentinel-1 and SAR constellation era. In Proceedings of the IGARSS 2019–2019 IEEE International Geoscience and Remote Sensing Symposium, Yokohama, Japan, 28 July–2 August 2019; pp. 5465–5467.
16. Ramis, R.; Garcia, A.; Marrero, J.; la Cruz-Reyna, D.; Carniel, R.; Vila, J. Volcanic and volcano-tectonic activity forecasting: A review on seismic approaches. *Ann. Geophys.* **2019**, *62*. [CrossRef]
17. Ren, C.X.; Peltier, A.; Ferrazzini, V.; Rouet-Leduc, B.; Johnson, P.A.; Brenguier, F. Machine learning reveals the seismic signature of eruptive behavior at Piton de la Fournaise volcano. *Geophys. Res. Lett.* **2020**, *47*, e2019GL085523. [CrossRef] [PubMed]
18. Carniel, R.; Guzman, S.R. Machine learning in volcanology: A review. In *Volcanoes—Updates in Volcanology*; IntechOpen: Rijeka, Croatia, 2021.
19. Amato, E.; Corradino, C.; Torrisi, F.; Del Negro, C. A Deep convolutional neural network for detecting volcanic thermal anomalies from satellite images. *Remote Sens.* **2023**, *15*, 3718. [CrossRef]

20. Ramsey, M.S.; Corradino, C.; Thompson, J.O.; Leggett, T.N. Statistical retrieval of volcanic activity in long time series orbital data: Implications for forecasting future activity. *Remote Sens. Environ.* **2023**, *295*, 113704. [CrossRef]
21. Corradino, C.; Malaguti, A.B.; Ramsey, M.S.; Del Negro, C. Quantitative Assessment of Volcanic Thermal Activity from Space Using an Isolation Forest Machine Learning Algorithm. *Remote Sens.* **2024**, *16*, 2001. [CrossRef]
22. Marzban, P.; Bredemeyer, S.; Walter, T.R.; Kästner, F.; Müller, D.; Chabrillat, S. Hydrothermally altered deposits of 2014 Askja landslide, Iceland, identified by remote sensing imaging. *Front. Earth Sci.* **2023**, *11*, 1083043. [CrossRef]
23. Anzieta, J.C. Application of Data Analysis and Machine Learning Techniques to Improve Baseline Volcano and Mountain Hazards Monitoring. Ph.D. Thesis, Simon Fraser University, Burnaby, BC, Canada, 2024.
24. Andaru, R.; Rau, J.Y.; Syahbana, D.K.; Prayoga, A.S.; Purnamasari, H.D. The use of UAV remote sensing for observing lava dome emplacement and areas of potential lahar hazards: An example from the 2017–2019 eruption crisis at Mount Agung in Bali. *J. Volcanol. Geotherm. Res.* **2021**, *415*, 107255. [CrossRef]
25. Anantrasirichai, N.; Biggs, J.; Albino, F.; Bull, D. A deep learning approach to detecting volcano deformation from satellite imagery using synthetic datasets. *Remote Sens. Environ.* **2019**, *230*, 111179. [CrossRef]
26. Biggs, J.; Anantrasirichai, N.; Albino, F.; Lazecky, M.; Maghsoudi, Y. Large-scale demonstration of machine learning for the detection of volcanic deformation in Sentinel-1 satellite imagery. *Bull. Volcanol.* **2022**, *84*, 100. [CrossRef] [PubMed]
27. Hajian, A.; Cannavò, F.; Greco, F.; Nunnari, G. Classification of Mt Etna (Italy) volcanic activity by machine learning approaches. *Ann. Geophys.* **2019**, *62*, VO231. [CrossRef]
28. Manley, G.F.; Mather, T.A.; Pyle, D.M.; Clifton, D.A.; Rodgers, M.; Thompson, G.; Londono, J.M. A deep active learning approach to the automatic classification of volcano-seismic events. *Front. Earth Sci.* **2022**, *10*, 807926. [CrossRef]
29. Falcin, A.; Métaxian, J.P.; Mars, J.; Stutzmann, É.; Komorowski, J.C.; Moretti, R.; Malfante, M.; Beauducel, F.; Saurel, J.-M.; Dessert, C.; et al. A machine-learning approach for automatic classification of volcanic seismicity at La Soufrière Volcano, Guadeloupe. *J. Volcanol. Geotherm. Res.* **2021**, *411*, 107151. [CrossRef]
30. Messina, A.; Langer, H. Pattern recognition of volcanic tremor data on Mt. Etna (Italy) with KKAnalysis—A software program for unsupervised classification. *Comput. Geosci.* **2011**, *37*, 953–961. [CrossRef]
31. Witsil, A.J.; Johnson, J.B. Analyzing continuous infrasound from Stromboli volcano, Italy using unsupervised machine learning. *Comput. Geosci.* **2020**, *140*, 104494. [CrossRef]
32. Gaddes, M.E.; Hooper, A.; Bagnardi, M. Using machine learning to automatically detect volcanic unrest in a time series of interferograms. *J. Geophys. Res. Solid Earth* **2019**, *124*, 12304–12322. [CrossRef]
33. Romano, R. Succession of the volcanic activity in the Etnean area. In *Memorie della Società Geologica Italiana*; Società geologica italiana: Rome, Italy, 1982; Volume 23, pp. 27–48.
34. Chester, D.K.; Duncan, A.M.; Guest, J.E.; Kilburn, C.R.J. *Mount Etna—The Anatomy of a Volcano*; Chapman & Hall: London, UK, 1985.
35. Rittman, A. Mount Etna and the 1971 eruption—Structure and evolution of Mount Etna. *Philos. Trans. R. Soc. Lond. Ser. A Math. Phys. Sci.* **1973**, *274*, 5–16.
36. Guest, J.E. Styles of eruption and flow morphology on Mt Etna. In *Memorie della Società Geologica Italiana*; Società Geologica Italiana: Rome, Italy, 1982; Volume 23, pp. 49–73.
37. Branca, S.; Del Carlo, P. Types of eruptions of Etna volcano AD 1670–2003: Implications for short-term eruptive behaviour. *Bull. Volcanol.* **2005**, *67*, 732–742. [CrossRef]
38. Andronico, D.; Cannata, A.; Di Grazia, G.; Ferrari, F. The 1986–2021 paroxysmal episodes at the summit craters of Mt. Etna: Insights into volcano dynamics and hazard. *Earth-Sci. Rev.* **2021**, *220*, 103686. [CrossRef]
39. Coltelli, M.; Pompilio, M.; Del Carlo, P.; Calvari, S.; Pannucci, S.; Scribano, V. Eruptive activity. *Acta Vulcanol.* **1998**, *10*, 141–148.
40. Coltelli, M.; Del Carlo, P.; Pompilio, M. Eruptive activity. *Acta Vulcanol.* **2000**, *12*, 63–67.
41. Calvari, S.; Neri, M.; Pinkerton, H. Effusion rate estimations during the 1999 summit eruption on Mount Etna, and growth of two distinct lava flow fields. *J. Volcanol. Geotherm. Res.* **2003**, *119*, 107–123. [CrossRef]
42. Alparone, S.; Andronico, D.; Lodato, L.; Sgroi, T. Relationship between tremor and volcanic activity during the Southeast Crater eruption on Mount Etna in early 2000. *J. Geophys. Res. Solid Earth* **2003**, *108*, 2241. [CrossRef]
43. Tanguy, J.C. Les éruptions historiques de l'Etna: Chronologie et localisation. *Bull. Volcanol.* **1981**, *44*, 585–640. [CrossRef]
44. Salvi, F.; Scandone, R.; Palma, C. Statistical analysis of the historical activity of Mount Etna, aimed at the evaluation of volcanic hazard. *J. Volcanol. Geotherm. Res.* **2006**, *154*, 159–168. [CrossRef]
45. Acocella, V.; Neri, M. What makes flank eruptions? The 2001 Etna eruption and its possible triggering mechanisms. *Bull. Volcanol.* **2003**, *65*, 517–529. [CrossRef]
46. Branca, S.; De Beni, E.; Proietti, C. The large and destructive 1669 AD eruption at Etna volcano: Reconstruction of the lava flow field evolution and effusion rate trend. *Bull. Volcanol.* **2013**, *75*, 1–16. [CrossRef]
47. Branca, S.; De Beni, E.; Chester, D.; Duncan, A.; Lotteri, A. The 1928 eruption of Mount Etna (Italy): Reconstructing lava flow evolution and the destruction and recovery of the town of Mascali. *J. Volcanol. Geotherm. Res.* **2017**, *335*, 54–70. [CrossRef]
48. Barberi, F.; Carapezza, M.L.; Valenza, M.; Villari, L. The control of lava flow during the 1991–1992 eruption of Mt. Etna. *J. Volcanol. Geotherm. Res.* **1993**, *56*, 1–34. [CrossRef]

49. Allard, P.; Behncke, B.; d'Amico, S.; Neri, M.; Gambino, S. Mount Etna 1993–2005: Anatomy of an evolving eruptive cycle. *Earth-Sci. Rev.* **2006**, *78*, 85–114. [CrossRef]
50. Coltelli, M.; Marsella, M.; Proietti, C.; Scifoni, S. The case of the 1981 eruption of Mount Etna: An example of very fast moving lava flows. *Geochem. Geophys. Geosystems* **2012**, *13*. [CrossRef]
51. Branca, S.; Privitera, F.; Palio, O.; Turco, M. Prehistoric human presence on Mount Etna (Sicily), in relation to the geological evolution. *Ann. Geophys.* **2021**, *64*, VO542.
52. Acocella, V.; Behncke, B.; Neri, M.; D'Amico, S. Link between major flank slip and 2002–2003 eruption at Mt. Etna (Italy). *Geophys. Res. Lett.* **2003**, *30*. [CrossRef]
53. Behncke, B.; Neri, M. The July–August 2001 eruption of Mt. Etna (Sicily). *Bull. Volcanol.* **2003**, *65*, 461–476. [CrossRef]
54. Clocchiatti, R.; Condomines, M.; Guénot, N.; Tanguy, J.C. Magma changes at Mount Etna: The 2001 and 2002–2003 eruptions. *Earth Planet. Sci. Lett.* **2004**, *226*, 397–414. [CrossRef]
55. Barberi, F.; Brondi, F.; Carapezza, M.L.; Cavarra, L.; Murgia, C. Earthen barriers to control lava flows in the 2001 eruption of Mt. Etna. *J. Volcanol. Geotherm. Res.* **2003**, *123*, 231–243. [CrossRef]
56. Neri, M.; Acocella, V.; Behncke, B.; Maiolino, V.; Ursino, A.; Velardita, R. Contrasting triggering mechanisms of the 2001 and 2002–2003 eruptions of Mount Etna (Italy). *J. Volcanol. Geotherm. Res.* **2005**, *144*, 235–255. [CrossRef]
57. Tanguy, J.C.; Condomines, M.; Le Goff, M.; Chillemi, V.; La Delfa, S.; Patanè, G. Mount Etna eruptions of the last 2750 years: Revised chronology and location through archeomagnetic and 226 Ra-230 Th dating. *Bull. Volcanol.* **2007**, *70*, 55–83. [CrossRef]
58. Branca, S.; Vigliotti, L. Finding of an historical document describing an eruption in the NW flank of Etna in July 1643 AD: Timing, location and volcanic products. *Bull. Volcanol.* **2015**, *77*, 95. [CrossRef]
59. Branca, S.; Abate, T. Current knowledge of Etna's flank eruptions (Italy) occurring over the past 2500 years. From the iconographies of the XVII century to modern geological cartography. *J. Volcanol. Geotherm. Res.* **2019**, *385*, 159–178. [CrossRef]
60. De Beni, E.; Cantarero, M.; Neri, M.; Messina, A. Lava flows of Mt Etna, Italy: The 2019 eruption within the context of the last two decades (1999–2019). *J. Maps* **2021**, *17*, 65–76. [CrossRef]
61. Tarquini, S.; Nannipieri, L. The 10 m-resolution TINITALY DEM as a trans-disciplinary basis for the analysis of the Italian territory: Current trends and new perspectives. *Geomorphology* **2017**, *281*, 108–115. [CrossRef]
62. Proietti, C.; De Beni, E.; Coltelli, M.; Branca, S. The flank eruption history of Etna (1610–2006) as a constraint on lava flow hazard. *Ann. Geophys.* **2011**, *54*, 480–490. [CrossRef]
63. Corradino, C.; Amato, E.; Torrisi, F.; Calvari, S.; Del Negro, C. Classifying major explosions and paroxysms at Stromboli volcano (Italy) from space. *Remote Sens.* **2021**, *13*, 4080. [CrossRef]
64. Anzieta, J.C.; Ortiz, H.D.; Arias, G.L.; Ruiz, M.C. Finding possible precursors for the 2015 Cotopaxi volcano eruption using unsupervised machine learning techniques. *Int. J. Geophys.* **2019**, *2019*, 6526898. [CrossRef]
65. Syakur, M.A.; Khotimah, B.K.; Rochman, E.M.S.; Satoto, B.D. Integration k-means clustering method and elbow method for identification of the best customer profile cluster. In *IOP Conference Series: Materials Science and Engineering*; IOP Publishing: Bristol, UK, 2018; Volume 336, p. 012017.
66. El-Mandouh, A.M.; Abd-Elmegid, L.A.; Mahmoud, H.A.; Haggag, M.H. Optimized K-means clustering model based on gap statistic. *Int. J. Adv. Comput. Sci. Appl.* **2019**, *10*. [CrossRef]
67. Hasibuan, A.; Kembuan, D.R.; Manoppo, C.T.M.; Tinambunan, M.H. Optimization of K-Means algorithm in grouping data using the statistical gap method. *J. Intell. Decis. Support Syst.* **2023**, *6*, 112–120.
68. Kaufman, L.; Rousseeuw, P.J. *Finding Groups in Data: An Introduction to Cluster Analysis*; John Wiley & Sons: Hoboken, NJ, USA, 2009.
69. Mato, F.; Toulkeridis, T. An unsupervised K-means based clustering method for geophysical post-earthquake diagnosis. In Proceedings of the 2017 IEEE Symposium Series on Computational Intelligence (SSCI), Honolulu, HI, USA, 27 November–1 December 2017; pp. 1–8.
70. Azzaro, R.; Branca, S.; Gwinner, K.; Coltelli, M. The volcano-tectonic map of Etna volcano, 1:100,000 scale: An integrated approach based on a morphotectonic analysis from high-resolution DEM constrained by geologic, active faulting and seismotectonic data. *Ital. J. Geosci.* **2012**, *131*, 153–170.
71. Duncan, A.M.; Chester, D.K.; Guest, J.E. Mount Etna volcano: Environmental impact and problems of volcanic prediction. *Geogr. J.* **1981**, *147*, 164–178. [CrossRef]
72. Armienti, P.; Innocenti, F.; Petrini, R.; Pompilio, M.; Villari, L. Sub-aphiric alkali basalts from Mt. Etna: Inferences on the depth and composition of the source magma. *Rend. Soc. Ital. Mineral. Petrol.* **1988**, *43*, 877–891.
73. Corsaro, R.A.; Pompilio, M. Dynamics of magmas at Mount Etna. *Geophys. Monogr.-Am. Geophys. Union* **2004**, *143*, 91–110.
74. Lormand, C.; Harris, A.J.; Chevrel, M.O.; Calvari, S.; Gurioli, L.; Favalli, M.; Fornaciai, A.; Nannipieri, L. The 1974 west flank eruption of Mount Etna: A data-driven model for a low elevation effusive event. *Front. Earth Sci.* **2020**, *8*, 590411. [CrossRef]
75. Corsaro, R.A.; Branca, S.; De Beni, E.; Tanguy, J.C. Tales from Three 18th Century Eruptions to Understand Past and Present Behaviour of Etna. *Front. Earth Sci.* **2021**, *9*, 774361. [CrossRef]
76. Silvestri, O. XVI. The eruption of etna on the 29th of August 1875. *Lond. Edinb. Dublin Philos. Mag. J. Sci.* **1874**, *49*, 126–134. [CrossRef]

77. Bruce, P.M.; Huppert, H.E. Solidification and melting along dykes by the laminar flow of basaltic magma. In *Magma Transport and Storage*; John Wiley & Sons: Hoboken, NJ, USA, 1990; pp. 87–101.
78. Wadge, G. The variation of magma discharge during basaltic eruptions. *J. Volcanol. Geotherm. Res.* **1981**, *11*, 139–168. [CrossRef]